Electronic Supplementary Material (ESI) for Soft Matter.

Measurement of molecular mixing at a conjugated polymer interface by specular and off-specular neutron scattering

David James,[1] Anthony M. Higgins,[1,*] Paul Rees,[1], Mark Geoghegan,[2] M. Rowan Brown,[1] Shion-Seng Chang,[1], Dyfrig Môn,[1] Robert Cubitt, [3], Robert Dalgliesh,[4] and Philipp Gutfreund,[3]

1 College of Engineering, Swansea University, Fabian Way, Crymlyn Burrows, Swansea, SA1 8EN, Wales, United Kingdom
2 Department of Physics and Astronomy, University of Sheffield, Hounsfield Road, Sheffield, S3 7RH, United Kingdom
3 Institut Laue-Langevin, 71 avenue des Martyrs, 38000 Grenoble, France
4 ISIS , Rutherford Appleton Laboratory, Harwell Oxford, Didcot, OX11 OQX, United Kingdom

SUPPLEMENTARY INFORMATION

Model implementation and validation.

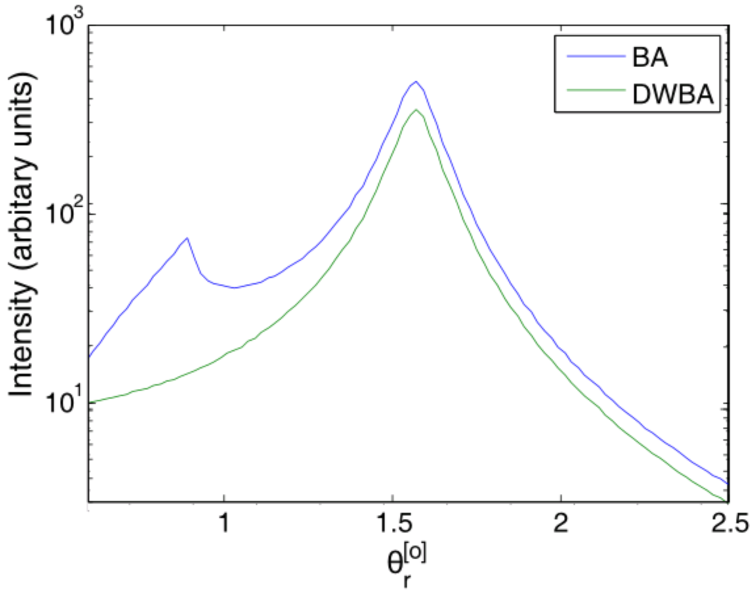

Figure S1; Comparison of the diffuse scattering using the Born Approximation (BA) and DWBA for a single rough interface between vacuum and a medium with scattering length density of 9.4 x 10^{-6} Å^{-2}, with interfacial roughness σ = 10Å, Hurst parameter h = 0.4 and lateral cut-off distance ξ = 7000 Å. The neutron wavelength is 8 Å and the incident angle θ_i = 1.5°. This is a repeat of a calculation performed by Pynn (Fig. 3(b))[1]

Fig. S1 shows a typical plot of off specular reflectivity as a function of θ_r using the Born approximation (BA) and distorted Wave Born Approximation (DWBA). The reflectivity calculated by the DWBA is a repeat of a calculation performed by Pynn (Fig. 3(b))[1]. The intensity of scattering at the angle of incidence and the fall-off in intensity for angles of reflection, θ_r, greater than the incident angle is very similar for both calculations. In the DWBA, Yoneda scattering with a peak in intensity at the critical angle of the inteface (~0.75°) is seen. Although the behaviour is very similar Fig. S1 does not exactly match Pynn's result[1] for the same value of h and ξ. In Pynn's work an approximation of the full expression is used, replacing the Fourier transform integral with a Voight function to eliminate the need for numerical calculation as it is the most computationally expensive part of the calculation. This assumption is only valid for a particular range of h. In our case the full expression is used in the calcuation of the off-specular reflectivity and evaluated numerically. To check the robustness of the calculation of the integral two different numerical schemes were used, the first using fast Fourier transforms (FFT) and the second Lobatto quadrature numerical integration. The FFT approach was applied to the full expression under the integral and also to the first ten terms of its Taylor series expansion as described by Sinha et al [2]. Each term of the expansion is evaluated as a separate transform. Each transform of the Taylor series components is much more computationally efficient to evaluate than the transform for the full expression. The quadrature method was only applied to the full expression. The FFT method involved evaluating the integral over a range of x such that the required q_x value of a pixel in the θ_r-λ map fell in the range of the computed frequency domain. The value of the integral for each pixel was assumed to occur at the q_x value in the frequency domain plot that was most closely matched to the q_x value of the pixel. Care was taken to choose a sampling frequency and number of points for the transform to make sure that in the required q_x range the transform gives a good approximation of the integral and that the values of q_x were not spread to far apart while maximising computational efficiency. Though a range of values is calculated for the FFT method and only a single value in the quadrature method, due to the efficiency of the FFT algorithm it is considerably faster than the quadrature method. Fig. S3 shows the results of the three methods of evaluating the integral for different values of h and ξ. The intensity and overall shape of the curves are very similar, for all integration methods used. However the smoothness of the curves calculated using the both the quadrature method and the Taylor series expansion evaluated by FFT are poor for low h values. The high gradient of the curve at low h could explain why both these methods begin to fail. The Taylor series does not contain enough terms to accurately describe the slope of the curve. With the quadrature method the approximation of the curve used over each interval is poorly representative of the actual curve. For this reason the FFT method evaluating the full expression was used throughout this work.

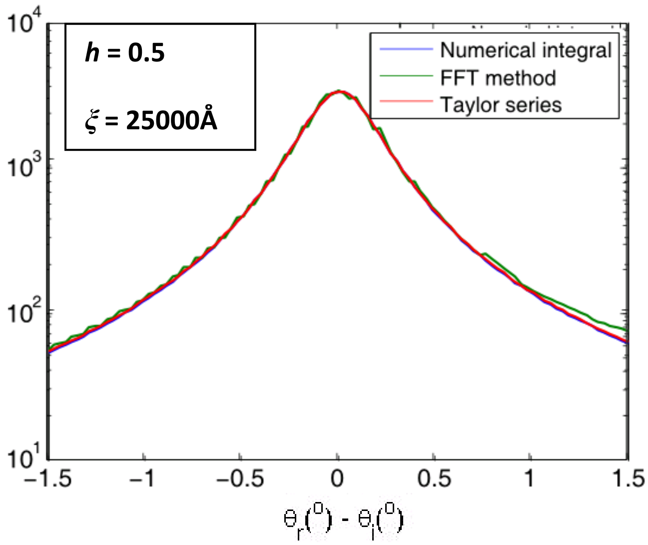

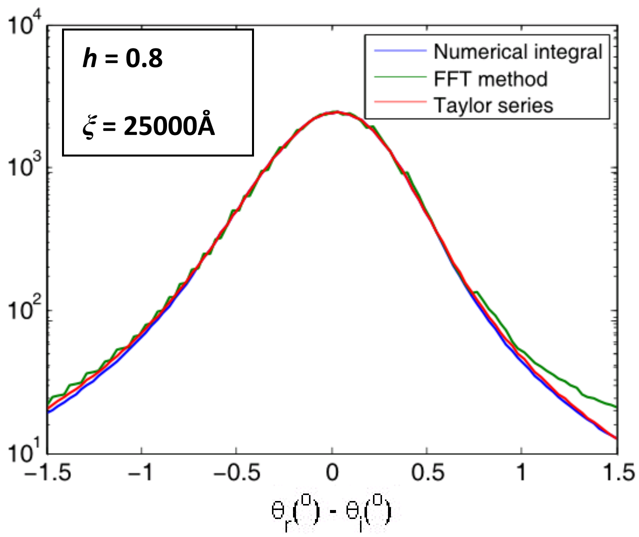

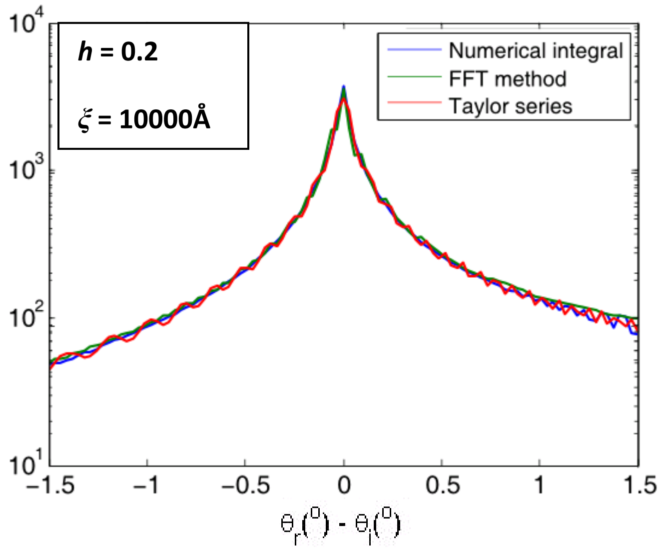

Figure S2; Comparison of three different numerical techniques used to evaluate the Fourier transform integral in Pynn (equation 22a)[1] for a single interface, with lateral roughness parameterised by various different values of the Hurst parameter, h, and the lateral cut-off length , ξ . The intensity (y axis) has arbitrary units.

Fitting algorithm.

The differential evolution algorithm minimises χ^2 by populating parameter space with a series of initial starting points. The algorithm then steps through successive generations in which each member of the population is mutated by combination with other, randomly selected, population members[3]. In all of the fits presented in the main paper (on silicon with rms roughness of 4.3 Å), all population members converged on the same minimum.

AFM on silicon substrates

Fig. S3 shows a typical trace and retrace height image of a silicon substrate used in the study.

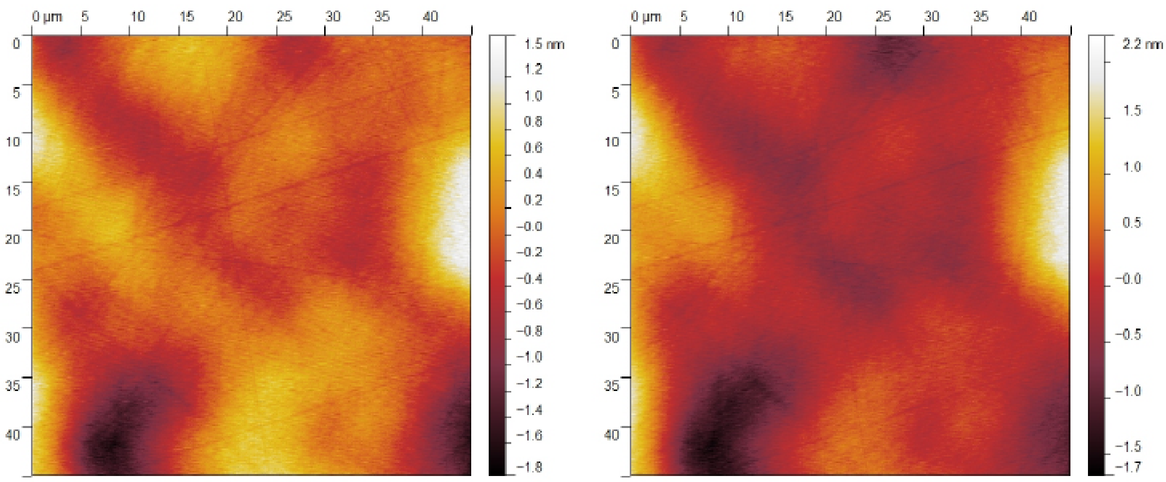

Figure S3; Contact mode AFM scan on a silicon substrate (<111> orientation Compart Technology).

Model robustness

To investigate the robustness of our findings we carried out a series of different fitting methodologies. These were i) the inclusion or absence of a silicon-oxide layer into both the specular and combined specular/off-specular fits, ii) an investigation into the sensitivity of our findings to the prefactor in the model that scales the diffuse scattering with-respect-to the true specular reflectivity and iii) the sensitivity of our findings to the value of the lateral cut-off, ξ, at the F8/dPMMA interface. These investigations are described in turn below.

Inclusion of a silicon-oxide layer;

Fits of the specular reflectivity without a silicon-oxide layer are shown in Fig. S4 (a). By comparing these fits with Fig. 2 (a), it is clear that the inclusion of an oxide layer results in significantly better fits, for higher q, for many of the different thickness bilayers. Several different sets of fits were performed. Within each set the silicon-oxide parameters were fixed. Fig. S4 (b) compares the interfacial roughness parameters from Fig. 2 (a) with the parameters from two sets of fits with different values of the silicon-oxide/dPMMA interface roughness. The overall behaviour of the fitted interfacial roughness parameters versus dPMMA film thickness is not strongly affected by the silicon-oxide layer parameters. The off-specular and combined specular/off-specular fits presented in the main paper contain no silicon-oxide layer. We also performed a set of combined specular/off-specular fits in which a silicon-oxide layer was included in the model. The silicon-oxide was modelled by adding an extra layer, between the silicon substrate and the dPMMA layer, in which the lateral cut-off, ξ, Hurst parameter, h, and roughness, σ_{lat}, were constrained to be the same at the silicon/silicon-oxide interface and at the silicon-oxide/dPMMA interface. The inclusion of such a layer, described by three adjustable parameters (the SLD; which was allowed to vary between that of pure silicon and SiO_2, the thickness; which was allowed to vary between 0 and 25 Å and the roughness; which was allowed to vary between 0 and 5 Å), into the model had very little effect on the fits. Examples of the fitted reflectivity maps are shown in Fig. S5, with fit parameters given in Table S1. The reflectivity maps are very similar to those in Fig. 3, and the fit parameters in Table S1 are very similar to those shown in Table 1 or plotted in Fig. 4.

Sensitivity to the prefactor in the model that scales the diffuse scattering with-respect-to the true specular reflectivity (the scaling factor);

The off-specular fits and the combined specular/off-specular fits in the main paper were performed with the scaling factor set equal to the value obtained from fitting the off-specular scattering from a single dPMMA layer. Table S2 gives the F8/dPMMA interface fit parameters obtained when this constraint is relaxed and the scaling factor is allowed to vary when fitting the off-specular data from each sample. Table S2 shows that the scaling factor obtained from these fits is of the same order as that from the dPMMA single layer fit. The behaviour of the extracted fit parameters as a function of dPMMA film thickness is not strongly affected by whether the scaling parameter is fixed at the value found for the dPMMA single layer or is allowed to vary.

Sensitivity to the value of the lateral cut-off, ξ, at the F8/dPMMA interface;

Table 1 shows that the lateral cut-off, ξ, at the F8/dPMMA interface for the three thickest dPMMA-layer samples is significantly different in the off-specular-only fits and the combined specular/off-specular fits. To examine the sensitivity of our results with-respect to ξ, we also performed combined specular/off-specular fits for two of these samples, in which the lateral cut-off at the F8/dPMMA interface was held fixed at the value from the off-specular-only fits. The results (see Table S3) show that similar values for the other F8/dPMMA interface fit parameters (the total and lateral roughness and the Hurst parameter) are obtained in the cases where the lateral cut-off is fixed or is allowed to vary.

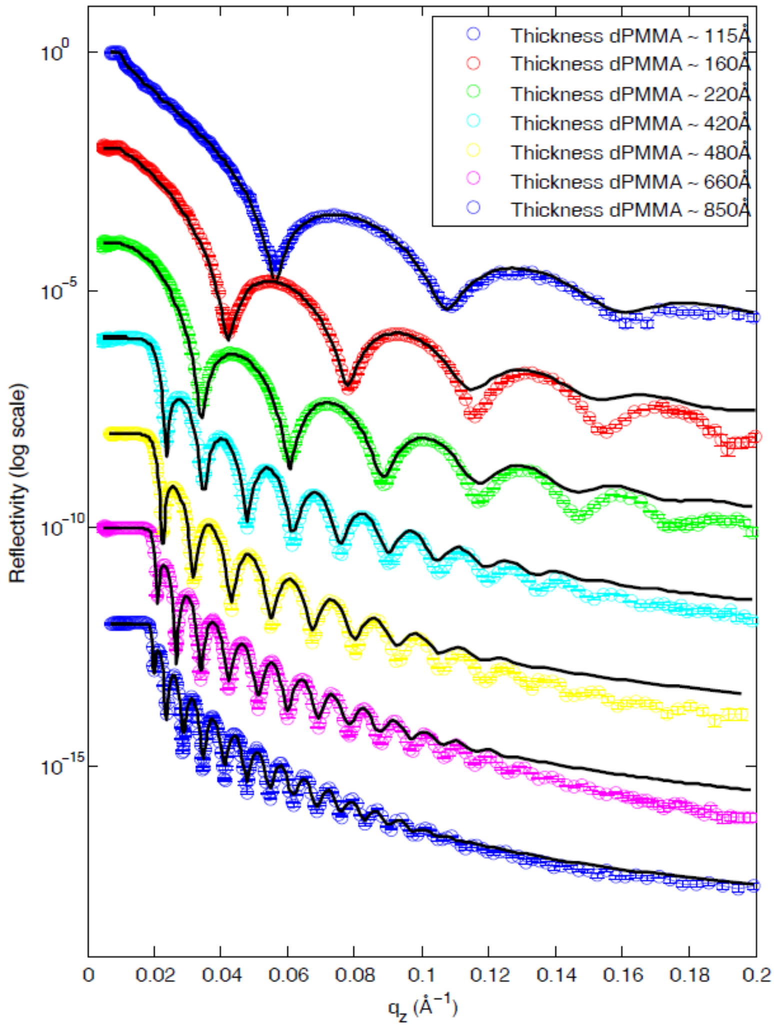

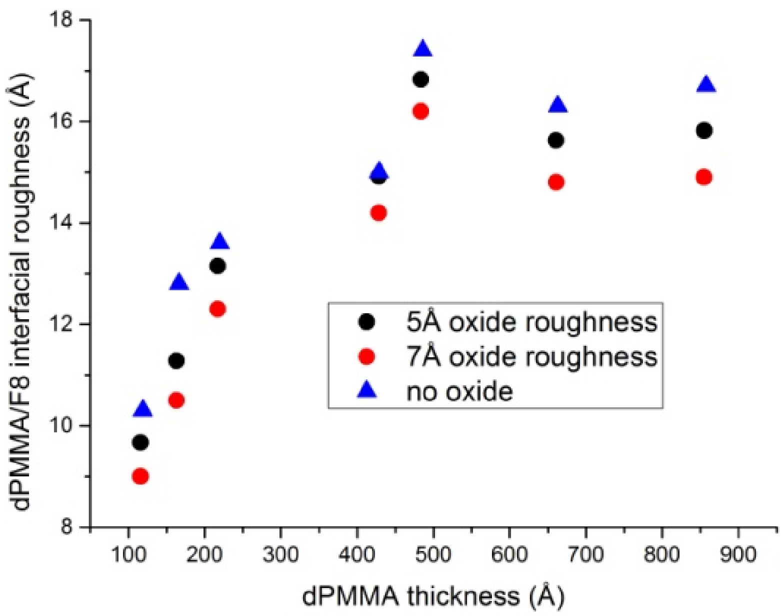

Figure S4; (a) Specular reflectivity and fits for dPMMA/F8 bilayers annealed at 180 °C for 3 hours. All fits were carried-out without an oxide layer. Curves are offset with-respect-to the y-axis for clarity. (b) Roughness of the dPMMA/F8 interface obtained from the fits to the specular reflectivity curves in Fig. S4 (a) (blue triangles) in comparison with roughness parameters for fits with silicon-oxide layers of thickness 9Å and roughness of either 5Å or 7Å (the roughness at the silicon/silicon-oxide interface was set to zero in both of these cases).

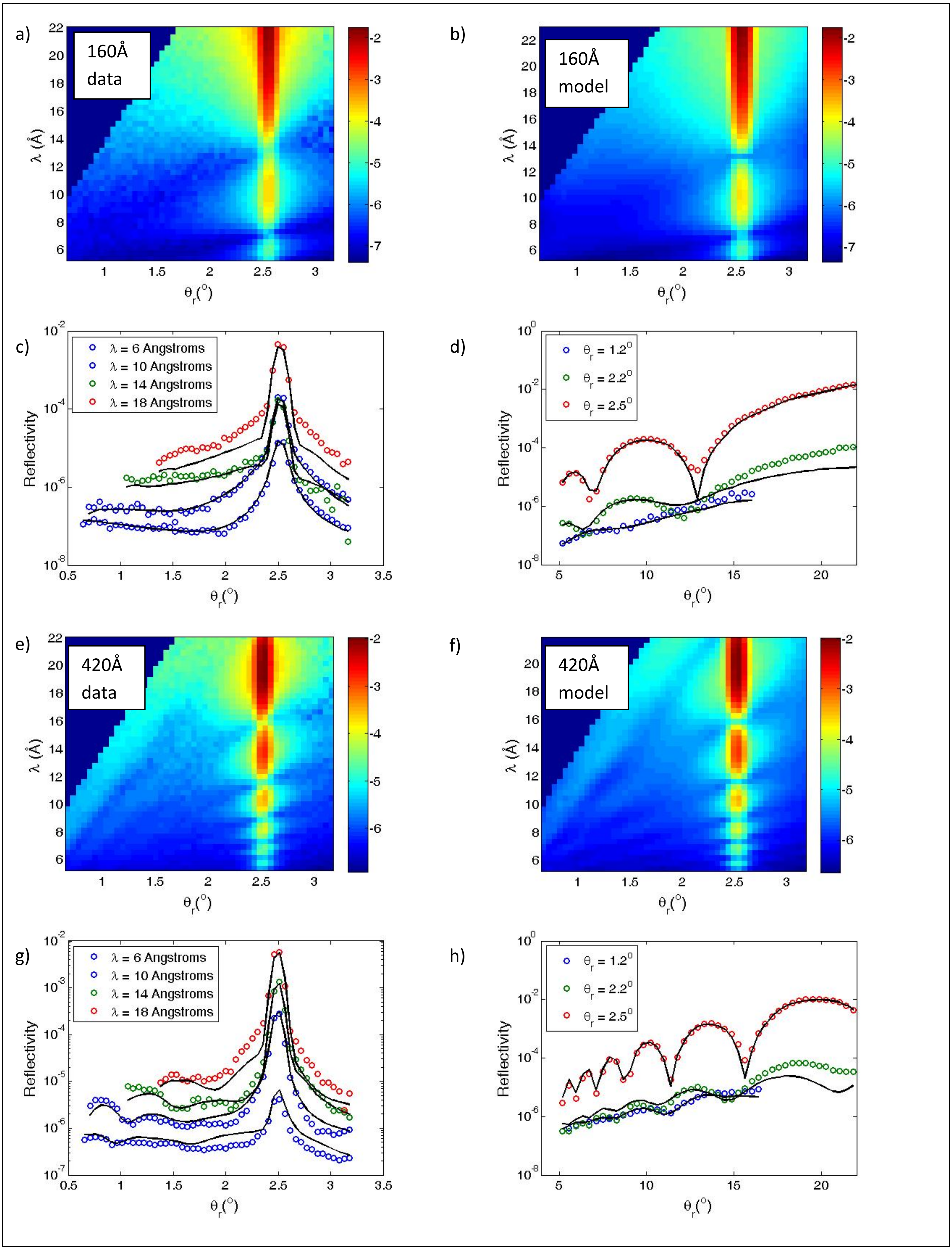

Figure S5; Fits with a silicon-oxide layer included. Experimental reflectivity data (a) and fitted reflectivity (b) for a sample with 1000Å F8 on 160Å dPMMA. Experimental reflectivity data (c) and fitted reflectivity (d) for a sample with 1000Å F8 on 420Å dPMMA. Figs (e) and (f) compare constant-wavelength and constant-reflected-angle cuts respectively, through the data (a) and the fit (b). Figs (g) and (h) compare constant-wavelength and constant-reflected-angle cuts respectively, through the data (c) and the fit (d).

	Sample 1	Sample 2	Sample 3	Sample 4	Sample 5
dPMMA thickness (Å)	161.4	214.6	423.1	480.7	648.0
σ_{tot}, F8/dPMMA interface (Å)	16.43	17.41	18.09	21.89	26.36
σ_{lat}, F8/dPMMA interface (Å)	10	10.35	15.33	14.89	24.68
σ_i, F8/dPMMA interface (Å)	13.03	13.99	9.6	16.05	9.26
Hurst parameter,*h*, , F8/dPMMA interface	0.5	0.57	0.17	0.19	0.14
Lateral cut-off, ξ, at the F8/dPMMA interface (μm)	1.6	1.3	0.75	0.87	2.6
Silicon-oxide thickness (Å)	22	24	6	21	25
Silicon/silicon-oxide (and silicon-oxide/dPMMA) roughness (Å)	4.7	4.6	2.8	3.0	5.0
Silicon-oxide SLD ($Å^{-2}$)	2.47×10^{-6}	2.52×10^{-6}	2.54×10^{-6}	3.18×10^{-6}	2.66×10^{-6}

Table S1; Fit parameters for combined specular/off-specular fits for the five bilayer samples with 100nm F8 on various thicknesses of dPMMA, with allowance for a thin silicon-oxide layer between the silicon substrate and the dPMMA layers. The perpendicular cut-off, $\xi_{\perp,jk}$, (parameterising the vertical correlation between the dPMMA/F8 interface and the silicon /dPMMA interface) was much larger than the dPMMA film thickness in all fits.

	Sample 1	Sample 2	Sample 3	Sample 4	Sample 5
dPMMA thickness (Å)	161 (162)	215 (215)	419 (419)	480 (481)	650 (650)
σ_{tot}, F8/dPMMA interface (Å)	26.0 (20.6)	22.7 (20.7)	31.2 (30.2)	29.3 (27.7)	30.4 (28.6)
σ_{lat}, F8/dPMMA interface (Å)	10.1 (13.1)	9.7 (13.3)	27.9 (29.1)	22.4 (20.7)	26.0 (25.5)
σ_i, F8/dPMMA interface (Å)	24.0 (16.0)	20.5 (15.9)	14.0 (8.3)	18.9 (16.8)	15.8 (12.9)
Hurst parameter,*h*, , F8/dPMMA interface	0.69 (0.61)	0.65 (0.60)	0.15 (0.10)	0.32 (0.21)	0.25 (0.20)
Lateral cut-off, ξ, at the F8/dPMMA interface (μm)	2.0 (1.7)	1.9 (1.5)	15.5 (7.1)	12.8 (11.3)	15.0 (6.0)
Scaling factor	0.14	0.12	0.05	0.052	0.059

Table S2; Fit parameters for off-specular-only fits for the five bilayer samples with 100nm F8 on various thicknesses of dPMMA, with the prefactor in the model that scales the diffuse scattering with respect to the true specular reflectivity (labelled scaling factor) allowed to vary. The perpendicular cut-off, $\xi_{\perp,jk}$, (parameterising the vertical correlation between the dPMMA/F8 interface and the silicon dPMMA interface) was much larger than the dPMMA film thickness in all fits. The figures in brackets are the fit parameters obtained when the scaling factor is fixed at the value from the single dPMMA layer fit (0.051).

	Sample 4		Sample 5	
ξ (μm)	11.3 (fixed)	0.5 (fitted)	6.0 (fixed)	2.0 (fitted)
dPMMA thickness (Å)	482.1	482.2	646.6	647.2
σ_{tot}, F8/dPMMA interface (Å)	23.4	22.2	27.1	26.5
σ_{lat}, F8/dPMMA interface (Å)	18.5	15.5	25.3	25.7
σ_i, F8/dPMMA interface (Å)	14.4	15.9	9.6	6.4
Hurst parameter, h, , F8/dPMMA interface	0.1	0.18	0.14	0.12

Table S3; Comparison between the fit parameters obtained from combined specular/off-specular fits in which the lateral cut-off at the F8/dPMMA interface, ξ, is either i) fixed at the value extracted from the off-specular only fit or ii) allowed to vary in the fits.

Off-specular scattering from silicon substrates with lower rms roughness

Fig. S6 shows the scattering from a dPMMA/F8 bilayer and from a single dPMMA layer, both on silicon substrates with rms roughness of 1.6 Å. The maps show Yoneda scattering but no lines of higher intensity along constant q_z contours. Attempts to extract lateral and intrinsic roughness parameters for the F8/dPMMA interface from this data using the same methodology applied to the data sets presented in the main paper were not successful. For the data sets in Fig. S5 the fitting algorithm did not converge on a single minimum from the multiple initial starting points. Instead, the fitting process resulted in possible solutions that were located in different local minima in parameter space. This occurred for both the single layer and bilayer fits, and resulted in potentially plausible fits with a very broad range of values for both the lateral and intrinsic roughness at the F8/dPMMA interface. The most plausible explanation for this is that the lack of significant scattering along lines of constant q_z, leaves the data sets over-parameterised by the model, leading to a spread of possible model solutions. It seems paradoxical, but the lower roughness of the silicon, which one might naively anticipate would give enhance sensitivity to the polymer-polymer interface, in fact does the opposite, by eliminating much of the off-specular scattering that could be utilised to further constrain the model fitting process.

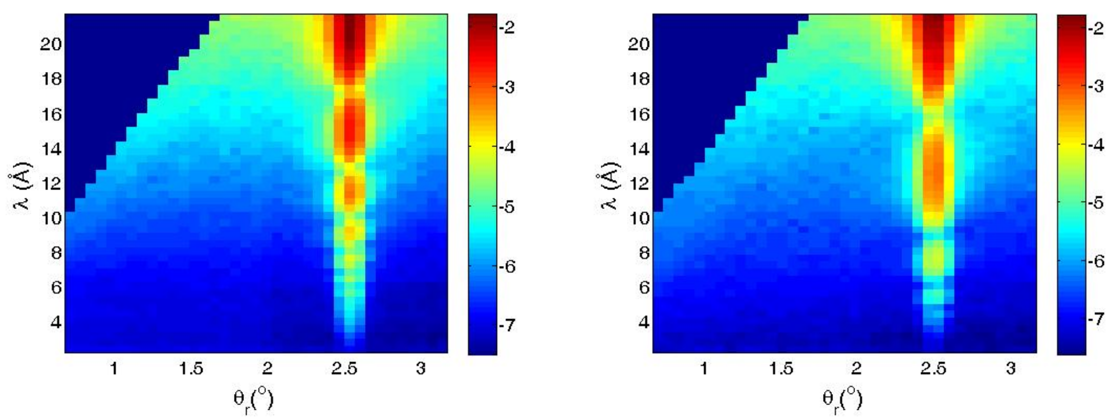

Figure S6; Experimental data showing specular and off-specular scattering from samples fabricated on silicon substrates (<111> orientation from Prolog Semicor, Ukraine) with rms roughness of 1.6 Å; (a) A dPMMA single layer of thickness 480 Å. (b) A dPMMA/F8 bilayer with layer thicknesses of 1000 Å and 220 Å respectively. Both samples were annealed at 180 ^{o}C for 3 hours.

REFERENCES FOR THE SUPPLEMENTARY MATERIAL

1. R. Pynn, Physical Review B **45** (2), 602-612 (1992).
2. S. Sinha, in *Synchrotron Techniques in Interfacial Electrochemistry*, edited by C. Melendres and A. Tadjeddine (Springer Netherlands, 1994), Vol. 432, pp. 85-95.
3. R. Storn and K. Price, Journal of Global Optimization **11** (4), 341-359 (1997).